A Quasi-Three-Dimensional Large-Signal Dynamic Model of Distributed Feedback Lasers

S. F. Yu

Abstract— **A simple, but powerful, quasi-three-dimensional large-signal dynamic model of distributed feedback semiconductor laser is presented. The transient response of lasers is analyzed by using a combined beam propagation method and time-domain algorithm that is capable of including the longitudinal and lateral variation of the optical-mode and carrier density profiles. In addition, the spontaneous emission noise, the nonuniform current injection resulting from the variation of Fermi-voltage as well as that of the refractive index distribution are also taken into consideration. Using this model, the influence of nonuniform waveguide structure on the static and dynamic responses of distributed feedback lasers is analyzed. In addition, a novel double tapered waveguide distributed feedback laser is proposed for stable single-mode operation at high power.**

I. Introduction

DISTRIBUTED feedback (DFB) lasers are key components in long-haul high-bit-rate lightwave transmission systems. This is because the DFB lasers demonstrate stable and single-mode operation. The mode stability of these devices, however, is crucially determined by a considerable number of parameters describing the nonlinear interaction between the carrier concentration and photon densities, which are lateral and longitudinal inhomogeneously distributed inside the cavity. Recently, number of models have been developed for the analysis of combined lateral and longitudinal spatial hole burning effects on the modulation response of the DFB lasers. It is shown that the lateral effects can have significant influence on the mode stability [1] as well as the modulation characteristic of DFB lasers [2], [3]. Their models include, with varying degrees of approximation on the optical field and carrier profile, the lateral variations of carrier concentration and refractive index profile arising from the carrier diffusion and stimulated recombination [1]–[3].

In this paper, we present a simple method for the calculation of large-signal transient responses of DFB lasers. The lateral and longitudinal variation of photon densities, carrier concentration as well as the refractive index distribution are determined self-consistently in a numerical manner. One major advantage of our dynamic model over the previous works is that the nonuniform waveguide structure [4], [5] can also be taken into calculation. In Section II, the coupled wave equations corresponding to the forward and reverse waves are derived from the time-dependent wave equation. The perturbation approximation and the effective index method are employed for the decomposition of transverse optical field. Section III describes the numerical technique used to obtain a self-consistent solution of the coupled wave equations and rate equation of carrier concentration. The dynamic behavior of DFB lasers with nonuniform waveguide structure is analyzed by the dynamic model and the results are given in Section IV. Finally, the results are summarized in Section V.

Manuscript received August 25, 1995; revised November 24, 1995. This work is supported by HKU CRCG, account code 337/062/0023.

The author is with the Department of Electrical and Electronic Engineering, University of Hong Kong, Pokfulam Road, Hong Kong.

Publisher Item Identifier S 0018-9197(96)02033-7.

II. Theory

The electric field E in the waveguide is governed by the wave equation given as

$$\left(\frac{\partial^2}{\partial x^2}+\frac{\partial^2}{\partial y^2}+\frac{\partial^2}{\partial z^2}\right)E=\frac{\varepsilon}{c^2}\frac{\partial^2 E}{\partial t^2}+\frac{1}{c^2}\frac{\partial \varepsilon}{\partial t}\frac{\partial E}{\partial t}, \tag{1}$$

where c is the velocity of light in free space and ε is the complex dielectric constant of the laser medium. The electric field E can be approximated by

$$E=\phi(x)E_t(y,\,z,\,t)e^{-j\omega t}, \tag{2}$$

where E_t is the slowly-varying electric field, j is a complex number, ω is the operating frequency, and ϕ is the normalized transverse field profile. From the wave equation (1), a set of coupled-wave equations for a resonant situation can be derived by combining the perturbation solution of the Floquet–Bloch expansion theory [6] and the conventional coupled-mode equations for the two guided waves. For a first-order grating, we take the longitudinal propagating field within the laser $E_t^{(0)}$ as

$$E_t^{(0)}(x,\,y,\,z,\,t)=[F(y,\,z,\,t)e^{-j\beta_o z}+R(y,\,z,\,t)e^{j\beta_o z}]\phi_o(x), \tag{3}$$

where F and R are the slowly varying longitudinal forward and reverse propagating field amplitudes and β_o is the propagation constant at the Bragg frequency. The effective index method [7] is used to reduce the three-dimensional wave equation to a two-dimensional wave in the y and z directions. We assume that the field profile in x direction satisfies

$$\frac{\partial^2\phi_o}{\partial x^2}+[k_o^2n_o^2(x,\,y)-\beta_{\text{eff}}^2]\phi_o=0, \tag{4}$$

where β_{eff} is the effective propagation coefficient in lateral direction and $n_o(x,\,y)$ is the refractive index distribution of the device. From above, the time-dependent coupled-wave equations for fields F and R are given by

$$\left(\frac{1}{\nu_g}\frac{\partial F}{\partial t}+\frac{\partial F}{\partial z}\right)=\left\{\frac{j}{2\beta_0}\frac{\partial^2}{\partial y^2}+(g+j\Delta\beta_{\text{eff}})\right\}F+j\kappa R+S_f, \tag{5a}$$

$$\left(\frac{1}{\nu_g}\frac{\partial R}{\partial t} - \frac{\partial R}{\partial z}\right) = \left\{\frac{j}{2\beta_0}\frac{\partial^2}{\partial y^2} + (g + j\Delta\beta_{\text{eff}})\right\} R + j\kappa F + S_r, \tag{5b}$$

where $2\Delta\beta_{\text{eff}}\beta_o = \beta_{\text{eff}}^2 - \beta_o^2$ and ν_g is the group velocity. g is the field gain and κ is the longitudinal coupling coefficient. The expression of κ is given by

$$\kappa = \frac{k_o^2}{2\beta_0}\int_{grating} A_0(x)\phi_o^2(x)\,dx, \tag{6}$$

where A_0 is the Fourier coefficient of the grating. Extra terms S_f and S_r are introduced to the coupled wave equations that represent the driving force of spontaneous noise coupled to the forward and reverse fields.

For quantum well active region, the field gain g is approximated by [5]

$$g(y, t) = \frac{1}{2}\left\{\Gamma_x a_N \log\frac{N}{N_o} - \alpha\right\}, \tag{7}$$

where Γ_x is the confinement factor in the transverse direction, a_N is the gain coefficient, N_o is the carrier concentration at transparency, α is the loss in the layers, and N is the carrier distribution inside the active region.

The derivation of Bragg condition $\Delta\beta_{\text{eff}}$ is given as

$$\Delta\beta_{\text{eff}} = \frac{\omega_o}{c} n_{\text{eff}}(y, z, t) - \frac{\pi}{\Lambda}, \tag{8}$$

where c is the speed of light and Λ is the pitch of the grating. n_{eff} is the effective refractive index in the lateral and longitudinal directions. Equation (8) takes into account the built-in index step along the lateral direction as well as the influence of carrier-induced index change inside the active region. n_{eff} can be written as

$$n_{\text{eff}} = \Gamma_x[n_b(y, z) + \Delta n_c], \tag{9}$$

where n_b is the built-in refractive index along the lateral direction, Δn_c is the change in refractive index induced by the carrier concentration and is approximated by

$$\Delta n_c = -\frac{\alpha_m\lambda_o}{4\pi}\frac{\partial g}{\partial N}\Delta N, \tag{10}$$

where α_m is the material linewidth enhancement factor and λ_o is the operation wavelength. ΔN is the small change of carrier concentration above threshold and $\partial g/\partial N$ is the differential gain.

The spontaneous noise coupled to the forward and reverse waves are introduced into calculation by adding S_f and S_r into coupled wave equations with the assumption that: 1) the spontaneous noise coupled to the forward and reverse fields have equal amplitude and 2) the spontaneous noise is uniform along the lateral direction. In our calculation, the spontaneous noise is generated from a Gaussian distributed random number generator [8] that satisfies the correlation

$$\begin{aligned}\langle S_i(z, t)S_i^*(z', t')\rangle &= \eta K R_{sp}\delta(t - t')\delta(z - z')/\nu_g\\ \langle S_i(z, t)S_i(z, t)\rangle &= 0,\end{aligned} \tag{11}$$

where $i = f, r$. Here, $R_{sp} = BN_{\text{ave}}^2/L$ is the bimolecular recombination per unit length contributed to spontaneous emission, η is the spontaneous coupling factor and K is the transverse Petermann factor. Also L is the length of laser and N_{ave} is defined as $N_{\text{ave}} = \int F\cdot N\cdot F^*\,dy/\int F\cdot F^*\,dy$.

The time-dependent rate equation of carrier concentration is given by

$$\frac{\partial N(y, z, t)}{\partial t} = \frac{J(N, t)}{eL_zN_w} - R(N) - \nu_g a_N \cdot\log\frac{N}{N_o}P + D\frac{\partial^2 N(y, z, t)}{\partial y^2}, \tag{12}$$

where L_z and N_w is the thickness and the number of quantum well, respectively. e is the electron charge, $J(N, t)$ is the current distribution and D is the diffusion constant. $R(N)$ is the total recombination rate of carrier concentration and is given by

$$R(N) = \frac{N}{\tau} + BN^2 + CN^3, \tag{13}$$

where τ is the carrier lifetime, B and C are bimolecular and Auger recombination coefficient, respectively. The photon density is given as

$$P = |F(y, z, t)|^2 + |R(y, z, t)|^2. \tag{14}$$

The injection current given in (12) can relate to the equivalent resistivity of p-layers ρ and is given by

$$J(N, t) = \frac{U - N_wU_F(N)}{\rho LW}, \tag{15}$$

where W is the width of the metal stripe, U is the applied voltage and U_F is the Fermi voltage in the quantum well layer. U_F can be approximated by [9]

$$U_F(N) = \frac{1}{q}\left(E_g + k_BT\cdot\ln\left\{\left[\exp\left(\frac{N}{N_c}\right) - 1\right]\cdot\left[\exp\left(\frac{N}{N_v}\right) - 1\right]\right\}\right), \tag{16}$$

where E_g is the energy gap between the first quantized energy level of conduction and valence bands of quantum well, k_B is the Boltzmann constant, and T is temperature in Kelvin. N_c and N_v are the effective conduction and valence edge density of states, respectively, and can be expressed as

$$\begin{aligned}N_{c/v} &= \frac{m_{e/h}^* k_BT}{\pi\hbar^2L_z}\\ &\approx 3.598\times 10^{16}\left(\frac{m_{e/h}^*\cdot T}{m_o}\right),\end{aligned} \tag{17}$$

where it is assumed $L_z = 100$ Å and $m_{e/h}^*$ is the effective mass of electron/hole.

III. Numerical Technique

The coupled-wave equations can be solved by using the time-domain algorithm [8] with the help of the beam propagation method [10]. The first-order difference approximation to

the partial differential on the left-hand side of (5) is given by

$$\left.\frac{\partial F}{\partial t}\right|_z \Delta t + \left.\frac{\partial F}{\partial z}\right|_t \Delta z = F(z+\Delta z, t+\Delta t) - F(z,t), \tag{18a}$$

$$\left.\frac{\partial R}{\partial t}\right|_z \Delta t - \left.\frac{\partial R}{\partial z}\right|_t \Delta z = R(z-\Delta z, t+\Delta t) - R(z,t). \tag{18b}$$

Using (18), (5) can be expressed as

$$\begin{bmatrix}\underline{\mathbf{F}}\\ \underline{\mathbf{R}}\end{bmatrix}_{z\pm\Delta z,\, t+\Delta t} = [\mathbf{M}]_{z,t}\begin{bmatrix}\underline{\mathbf{F}}\\ \underline{\mathbf{R}}\end{bmatrix}_{z,t} + \{j\kappa\cdot\Delta z\}\begin{bmatrix}\underline{\mathbf{R}}\\ \underline{\mathbf{F}}\end{bmatrix}_{z,t}, \tag{19}$$

where we have assumed $\Delta z = \nu_g \Delta t$. The laser cavity is divided into n segments of equal spacing $\Delta z = L/n$. $\underline{\mathbf{F}}$ and $\underline{\mathbf{R}}$ are vectors with m elements which represent the lateral variation of optical field from the middle of the waveguide ($y = 0$) to the side of the laser and at a particular longitudinal position (i.e., at a particular z). It must be noted that ν_g is nonuniformly distributed along the longitudinal direction due to the carrier induced index change. The variation of ν_g can be taken into consideration by allowing the change of Δz along the longitudinal direction such that $\Delta z/\nu_g = \Delta t =$ constant. However, our assumption on constant ν_g is still valid if the variation of n_{eff} is less than 0.1%.

The matrix $[\mathbf{M}]_{z,t}$ given in (19) is given by

$$[\mathbf{M}]_{z,t} = \{[\mathbf{I}] + [\mathbf{H}]\cdot\Delta z\}_{z,t}, \tag{20}$$

where $[\mathbf{I}]$ is a $m \times m$ identity matrix. In (20), the convergence of the calculation requires small Δz, however, we can apply the plane wave approximation on the lateral fields to improve the computing efficiency and the matrix $[\mathbf{M}]_{z,t}$ can be written as

$$[\mathbf{M}]_{z,t} = \{[\mathbf{I}] + [\mathbf{H}]\cdot\Delta z + \tfrac{1}{2}[\mathbf{H}]^2\cdot\Delta z^2 + \tfrac{1}{6}[\mathbf{H}]^3\cdot\Delta z^3 + \tfrac{1}{24}[\mathbf{H}]^4\cdot\Delta z^4 + \cdots\}_{z,t}. \tag{21}$$

$[\mathbf{H}]$ in (20) and (21) is a $m \times m$ matrix representing the operator H where

$$H = \frac{j}{2\beta_0}\frac{\partial^2}{\partial y^2} + (g + j\Delta\beta_{\text{eff}}). \tag{22}$$

Let $\psi^{\pm}$ be the qth element of the field vectors (i.e., $\underline{\mathbf{F}}$ and $\underline{\mathbf{R}}$), the derivatives in the operator H can be approximated by the finite difference

$$\left.\frac{\partial^2\psi^{\pm}}{\partial y^2}\right|_q = \frac{\psi^{\pm}_{q+1} - 2\psi^{\pm}_q + \psi^{\pm}_{q-1}}{\Delta y^2}, \tag{23}$$

where $q = 1$ to $m-1$. Because of the symmetry of the field, the second derivative at the middle of the waveguide (i.e., $y = 0$ or $q = 1$) takes the particular form

$$\left.\frac{\partial^2\psi^{\pm}}{\partial y^2}\right|_{q=1} = \frac{2(\psi^{\pm}_2 - \psi^{\pm}_1)}{\Delta y^2}. \tag{24}$$

Now, the elements of matrix $[\mathbf{H}]$ can be written as

$$H_{1,1} = -j/\Delta y^2\beta_o + j\Delta\beta_{\text{eff}} + g, \tag{25a}$$

$$H_{1,2} = j/\Delta y^2\beta_o, \tag{25b}$$

for $q > 1$,

$$H_{q,q-1} = j/2\Delta y^2\beta_o, \tag{26a}$$

$$H_{q,q} = -j/\Delta y^2\beta_o + j\Delta\beta_{\text{eff}} + g, \tag{26b}$$

$$H_{q,q+1} = j/2\Delta y^2\beta_o. \tag{26c}$$

Other matrix elements are zero. It is assumed that $\Delta y = W/2m$ and $\psi^{\pm} \to 0$ for $q \to$ large.

The iteration procedure is started with an arbitrary profile for both $\underline{\mathbf{F}}$ and $\underline{\mathbf{R}}$ at the facets. Then they are propagating back and forth until a required time step is obtained. The boundary conditions for the forward and reverse waves $\underline{\mathbf{F}}$ and $\underline{\mathbf{R}}$ at the facets can be written as

$$\underline{\mathbf{F}}_{z=0} = r_L\underline{\mathbf{R}}_{z=0}$$

and

$$\underline{\mathbf{R}}_{z=L} = r_R\underline{\mathbf{F}}_{z=L}, \tag{27}$$

where we have chosen $z = 0$ and L are the positions of the left-hand and right-hand facets, respectively. r_L and r_R are the amplitudes of facet reflections.

The carrier concentration N given in (12) is in fact a vector with m elements, (say $\underline{\mathbf{N}}$), representing the lateral distribution of carrier concentration at a particular longitudinal direction. The derivative of carrier concentration in (12) can be approximated by the finite difference

$$\left.\frac{\partial^2\underline{\mathbf{N}}}{\partial y^2}\right|_q \doteq \frac{N_{q+1} - 2N_q + N_{q-1}}{\Delta y^2}, \tag{28}$$

where N_q is an element of $\underline{\mathbf{N}}$. The time variation of carrier concentration can also be approximated by

$$\left.\frac{\partial\underline{\mathbf{N}}}{\partial t}\right|_q \Delta t = N_q(t+\Delta t) - N_q(t), \tag{29}$$

where Δt is identical to that used in (18) and the time variation of carrier concentration is synchronized with the traveling waves. Substitute (28) and (29) into (12), the rate equation of carrier concentration can be written as

$$N_q(t+\Delta t) - N_q(t) = \Delta t\left\{\frac{J(N_q,t)}{eL_zN_w} - R(N_q) - \nu_g a_N \log\frac{N_q}{N_o}P_q + D\frac{N_{q+1} - 2N_q + N_{q-1}}{\Delta y^2}\right\}. \tag{30}$$

In each time interval, Δt, (30) is solved subject to the conditions that N and its derivative are continuous everywhere and at the middle of the waveguide (i.e., $y = 0$ or $q = 1$), the

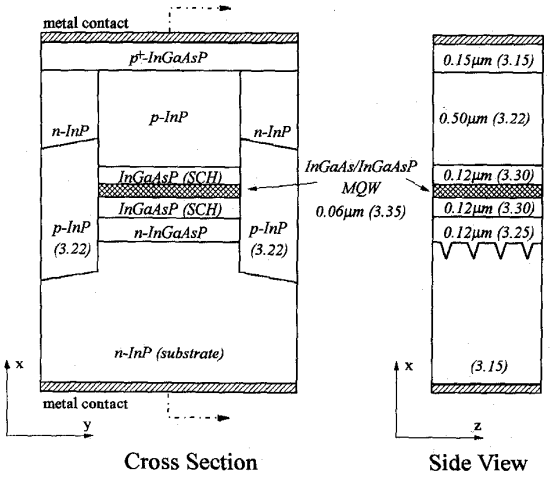

Fig. 1. Schematic cross section and side view of the DFB laser investigated in this paper.

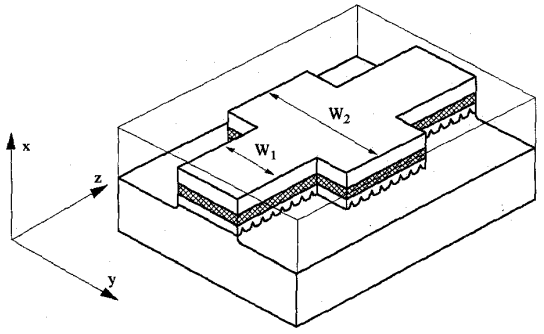

Fig. 2. Schematic structure of a phase adjusted DFB laser. W_1 and W_2 are the width of the waveguide and phase adjustment region.

second derivative takes the form

$$\left.\frac{\partial^2 \underline{\mathbf{N}}}{\partial y^2}\right|_{q=1} = \frac{2(N_2 - N_1)}{\Delta y^2}, \tag{31a}$$

and at rim of the waveguide (i.e., $y = W/2$ or $q = m-1$), the second derivative takes the form

$$\left.\frac{\partial^2 \underline{\mathbf{N}}}{\partial y^2}\right|_{q=m-1} = \frac{2(N_{m-2} - N_{m-1})}{\Delta y^2}. \tag{31b}$$

IV. Numerical Results

The basic structure used in our analysis is the buried heterostructure InGaAsP–InGaAs (1.55 μm) separate-confinement multi-quantum well (SCH-MQW) DFB lasers with first-order grating. A schematic of the device is shown in Fig. 1. The laser is composed of seven layers, the p^+-InGaAsP layer, p-InP buffer layer, the InGaAsP SCH layers, the InGaAsP–InGaAs multiquantum-well active layer, the n-InGaAsP guiding layer, and the n-InP substrate. The current blocking layers are of n-InP and p-InP material. It is assumed that the thickness of the barrier and well of the active region are both equal to 100 Å. The DFB laser has

TABLE I

Parameter	Symbol	Value
carrier lifetime in active layer	τ	3×10^{-9} s
Bimolecular carrier recombination coefficient	B	1×10^{-10}cm^{3}s^{-1}
Auger recombination rate	C	3×10^{-29}cm^{6}s^{-1}
gain coefficient	a_N	1500cm^{-1}
transparency carrier density	N_0	1.5×10^{18}cm^{-3}
scattering & absorption loss in waveguide	α	40 cm^{-1}
differential gain coefficient	$\partial g/\partial N$	4×10^{-16}cm^2
linewidth enhancement factor	α_m	3.0
diffusion constant	D	5cm^{2}s^{-1}
grating coupling coefficient	κ	20–40cm^{-1}
effective group velocity	v_g	8.11×10^9cms^{-1}
cavity length	L	600μm
thickness of quantum well	L_z	100Å
transverse confinement factor	Γ_x	0.0325
lasing wavelength	λ_0	1.55μm
left facet reflectivity	r_L	0
right facet reflectivity	r_R	0
equivalent resistance of p- and n- layers	ρ	80.0Ω
energy bandgap	E_g	1.35eV
effective mass of electron (InGaAs)	m_e	$0.066m_0$
effective mass of heavy hole (InGaAs)	m_h	$0.335m_0$
number of quantum well	N_w	2
spontaneous coupling factor	η	1×10^{-4}
Petermann factor	K	1
operational temperature	T	300°K

$\lambda/4$ phase shifted with both facets anti-reflection coated. In the following calculations, the device parameters used in the model are given in Table I.

A. Phase Adjusted Distributed Feedback Laser

$\lambda/4$ phase shifted can be introduced along the longitudinal direction of the waveguide through the phase adjustment region [11], [12]. Fig. 2 shows the schematic of waveguide structure of DFB lasers with wide phase adjustment region at the middle of the waveguide. In the calculations given below, the width of the waveguide (W_1) and phase adjustment region (W_2) is allowed to vary between 3–4 μm. This magnitude of stripe width is employed to illustrate the influence of lateral modes competition on the dynamic response of DFB lasers. We are going to demonstrate the utilization of phase adjustment region to control the longitudinal as well as lateral modes in DFB lasers.

Fig. 3 shows the switch-on transient response of DFB laser with wide phase adjustment region and κL is set to 1.2, 2.1, and 2.4. The width of the waveguide (W_1) and the phase adjustment region (W_2) is equal to 3 and 4 μm, respectively, and the corresponding length of the phase adjustment region is equal to 200 μm. The laser is initially biased at threshold and then modulated with a step current. The steady-state optical power from the anti-reflection facets is kept around 10 mW for comparison. It is shown in Fig. 3(c) that mode beating is observed nearly 0.9 ns after the switch-on of the laser. The corresponding steady-state optical spectra are also shown in Fig. 3. Mode beating is caused by the excitation of longitudinal side mode and this is confirmed by the steady-state carrier distribution along the active region as shown in Fig. 4. Lateral spatial hole burning is observed at the center of the stripe and

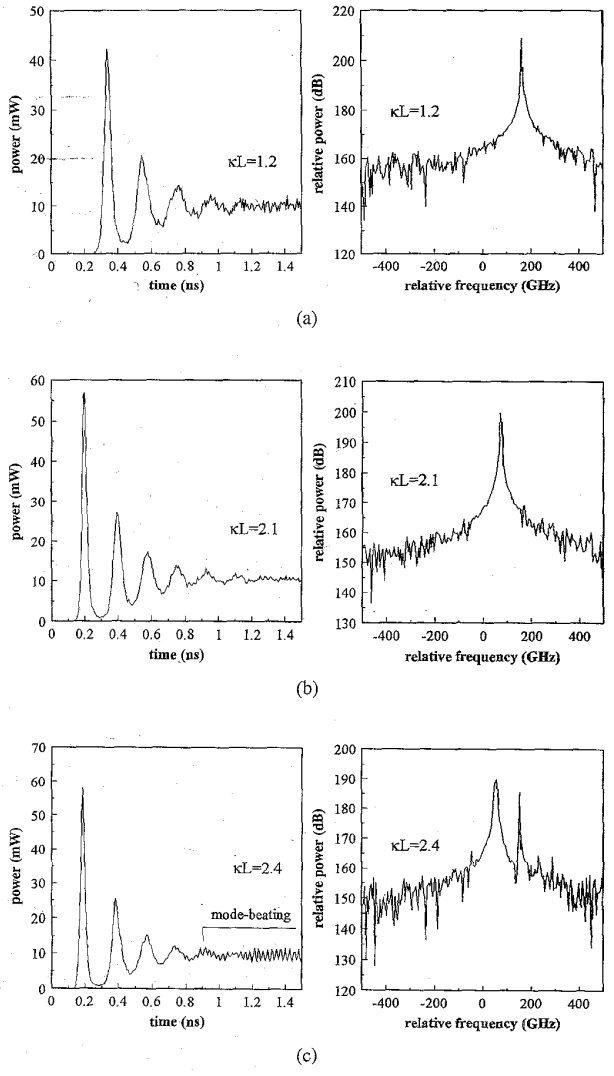

Fig. 3. The transient optical power response and steady-state spectra of DFB laser with wide phase adjustment region ($W_1 = 3\,\mu$m and $W_2 = 4\,\mu$m). (a) $\kappa L = 1.2$, (b) $\kappa L = 2.1$, and (c) $\kappa L = 2.4$.

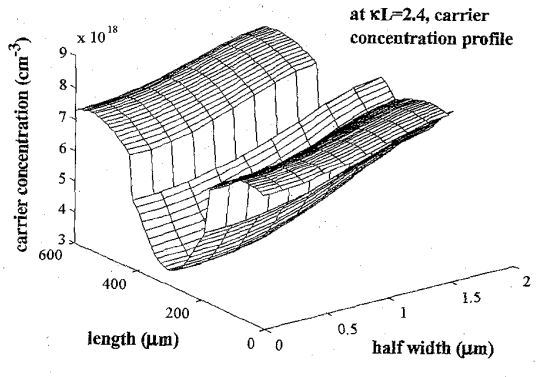

Fig. 4. The steady-state lateral and longitudinal carrier concentration distribution of DFB laser with wide phase adjustment region and $\kappa L = 2.4$.

there is no sight of first-order lateral mode. The excitation of the longitudinal mode is attributed to the enhancement of

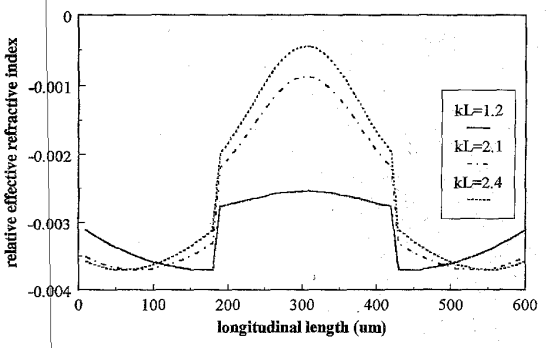

Fig. 5. The corresponding steady-state longitudinal effective refractive index profile (Δn_{eff}) of Fig. 3.

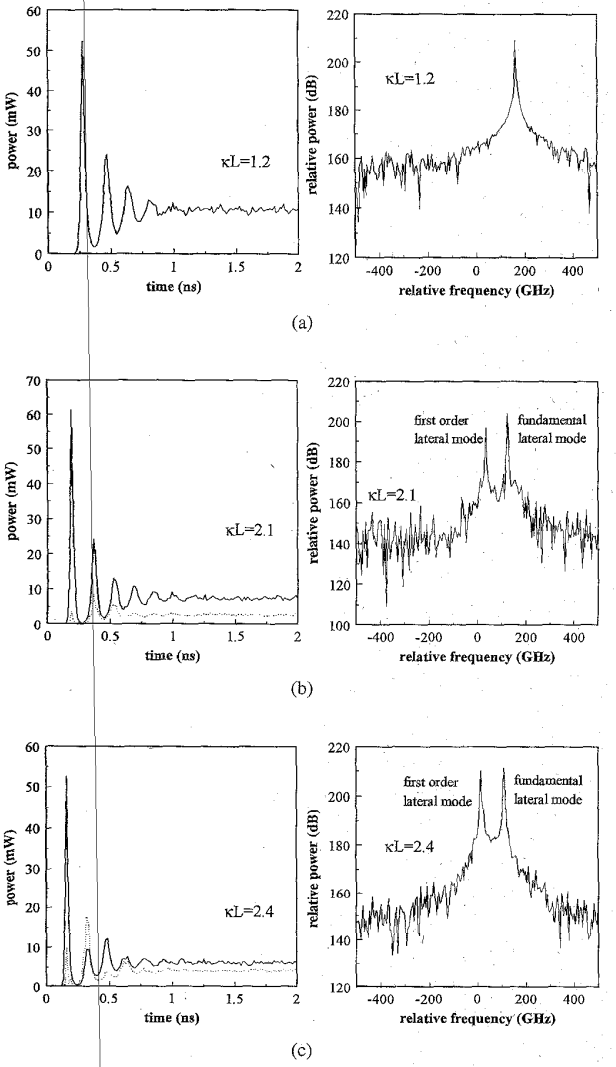

Fig. 6. The transient optical power response and steady-state spectra of DFB laser with narrow phase adjustment region ($W_1 = 4\,\mu$m and $W_2 = 3\,\mu$m). (a) $\kappa L = 1.2$, (b) $\kappa L = 2.1$, and (c) $\kappa L = 2.4$. Solid line—fundamental lateral mode, dotted line—first-order lateral mode.

longitudinal spatial hole burning for device with large κL. Fig. 5 shows the effective longitudinal index distribution of

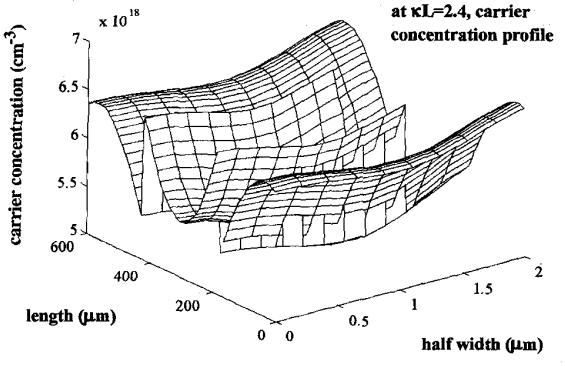

Fig. 7. The steady-state lateral and longitudinal carrier concentration distribution of DFB laser with narrow phase adjustment region and $\kappa L = 2.4$.

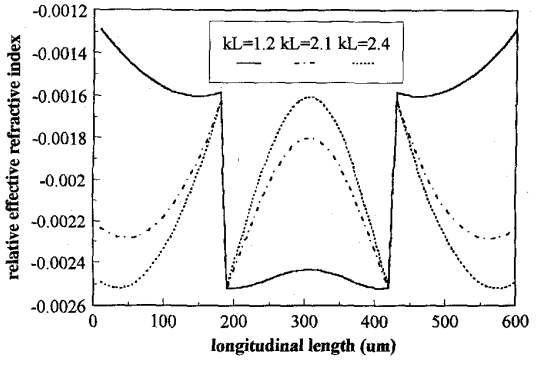

Fig. 8. The corresponding steady-state longitudinal effective refractive index profile (Δn_{eff}) of Fig. 6.

DFB laser at steady state for the cases of κL equal to 1.2, 2.1, and 2.4. The effective longitudinal refractive index Δn_{eff} is defined as

$$\Delta n_{\text{eff}} = \Gamma_x \int_{active} F \cdot \Delta n_c \cdot F^* \, dy \Big/ \int_{all} F \cdot F^* \, dy. \quad (32)$$

As shown in Figs. 4 and 5, severe spatial hole burning of carrier concentration as well as a step change of refractive index are exhibited at the phase adjustment region. The excitation of longitudinal side mode is caused by the nonuniform distribution of refractive index. On the other hand, lateral side mode is not observed in DFB laser with wide phase adjustment region. For devices with $\kappa L > 2.4$, the dynamic and static responses are similar to the case of $\kappa L = 2.4$ except mode beating is enhanced with the increase of κL.

$\lambda/4$ phase shifted can also be produced by phase adjustment region with width narrower than the waveguide. Fig. 6 shows the switch-on transient response of DFB laser with narrow phase adjustment region and κL equal to 1.2, 2.1, and 2.4. It is assumed that the width of the waveguide (W_1) and the phase adjustment region (W_2) is equal to 4 and 3 μm, respectively, and the corresponding length of the phase adjustment region is equal to 200 μm. In Fig. 6, the time evolution of the fundamental and first-order lateral modes are separated from the total field in order to indicate the influence of first-order lateral modes on the dynamic response of DFB laser. As we

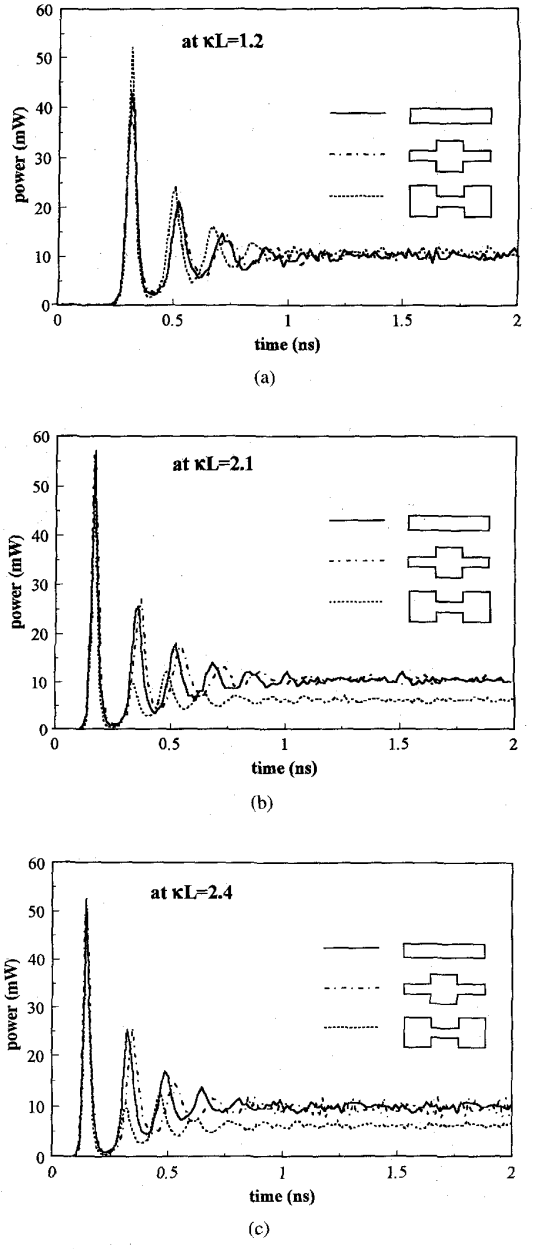

Fig. 9. Comparison between the transient output power response of DFB lasers with uniform waveguide and phase adjustment regions. (a) $\kappa L = 1.2$, (b) $\kappa L = 2.1$, and (c) $\kappa L = 2.4$.

can see first-order lateral mode is excited for κL larger than 1.2. The corresponding steady-state optical spectra are also shown in Fig. 6 for comparison. The carrier concentration of DFB laser for the case $\kappa L = 2.4$ is shown in Fig. 7. Severe lateral hole burning is observed away from the center of the waveguide and this is caused by the excitation of lateral side mode. In the above calculations, longitudinal side mode is not observed for all cases during the turn-on period of the current step. The reason can be explained by the longitudinal distribution of effective refractive index as shown in Fig. 8. As we can see the steady-state longitudinal spatial hole burning

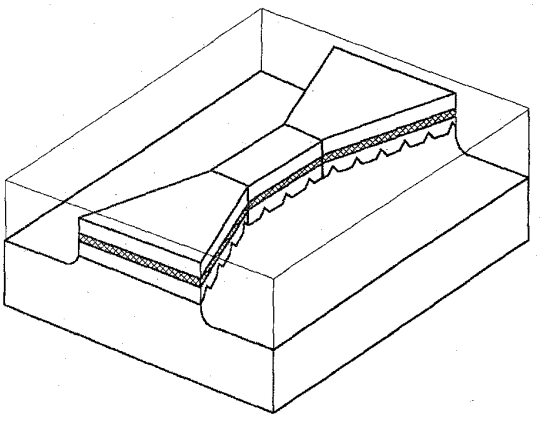

Fig. 10. Schematic of a DFB laser with double tapered waveguide structure.

is less severe that the case for DFB lasers with wide phase adjustment region. For devices with $\kappa L > 2.4$, the static and dynamic responses are similar to the case $\kappa L = 2.4$ except the lateral side mode is enhanced with the increase of κL.

Fig. 9 compares the transient response of DFB lasers with κL varies between 1.2–2.4. We analysis the $\lambda/4$ phase shifted DFB lasers with: 1) uniform stripe width, 2) wide, and 3) narrow phase adjustment region. As we can see relaxation oscillation frequency is enhanced for devices with large κL. In addition, the DFB lasers with narrow phase adjustment region exhibit larger relaxation oscillation frequency than that of devices with uniform stripe width or wide phase adjustment region.

It is shown that wide or narrow adjustment regions can provide sufficient longitudinal phase shifted, however, these methods may excite longitudinal and lateral side modes at high κL. For DFB lasers with wide phase adjustment region, stable single lateral mode can be maintained at large κL but longitudinal side modes are excited by the longitudinal spatial hole burning. On the other hand, longitudinal side mode is suppressed for devices with narrow phase adjustment region but lateral side mode is excited. In fact, single oscillation mode can be achieved in DFB with narrow phase adjustment region provided that the stripe width is less than 3 μm (only fundamental lateral mode is supported in waveguide with such dimension). However, it is also desired to have lasers with wide stripe width near the facets for the reason of high output power. In design of high power lasers, stripe width between 3–7 μm is commonly found [13], [14]. Therefore, the conventional phase adjusted DFB lasers may not satisfy for the application in high power and a DFB laser with novel waveguide structure is required for stable single-mode and high-output power operation.

B. Double Tapered Waveguide Distributed Feedback Laser

Fig. 10 shows the proposed waveguide structure of DFB lasers. The optical waveguide has double tapered structure with narrow phase adjustment region at the middle of the waveguide. The corresponding width of the waveguide near the facets and the phase adjustment region is equal to 4 and

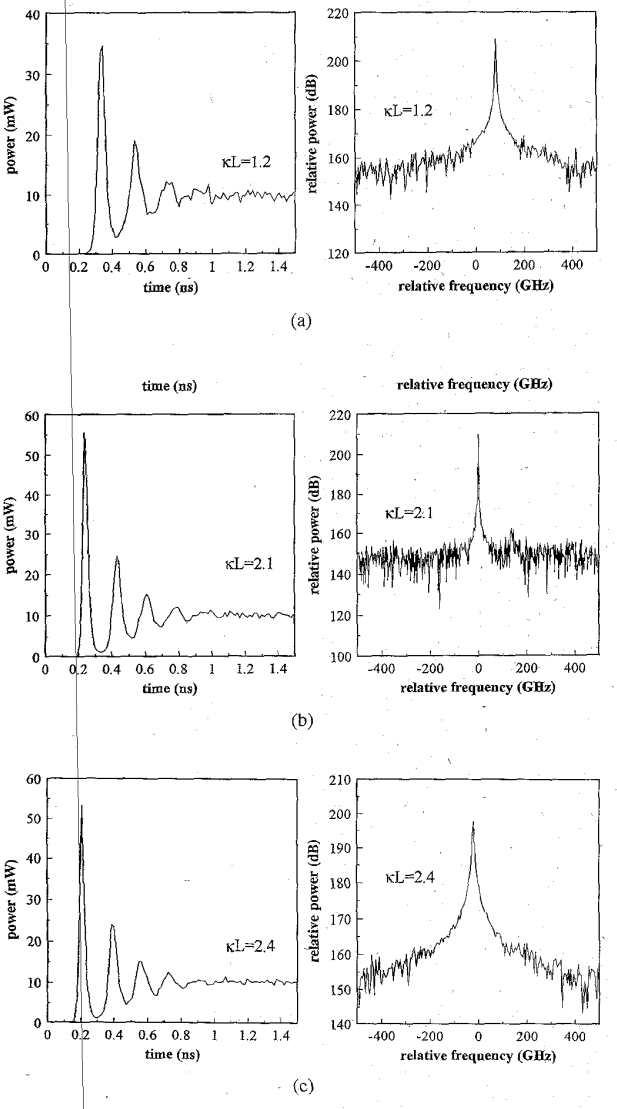

Fig. 11. The transient optical power response and steady-state spectra of DFB laser with double tapered waveguide structure. (a) $\kappa L = 1.2$, (b) $\kappa L = 2.1$, and (c) $\kappa L = 2.4$.

3 μm, respectively, and the length of the phase adjustment region is 200 μm. The tapered waveguide is designed to suppress lateral side mode and $\lambda/4$ phase shifted is produced by the narrow-phase adjustment region for single-longitudinal-mode oscillation. In addition, wide-stripe width reduces power density at the facets as well as enhancement of emitted power level.

Fig. 11 shows the dynamic response of DFB with double tapered waveguide for κL equal to 1.2, 2.1, and 2.4. It is clearly shown that this device structure can maintain stable single longitudinal and lateral mode at high power. The carrier concentration profile at steady state is shown in Fig. 12 for the case $\kappa L = 2.4$. It can be seen that the lateral spatial hole burning is observed at the center of the stripe and single lateral mode is also maintained by the tapered waveguide structure. The steady-state effective refractive index distribution of the

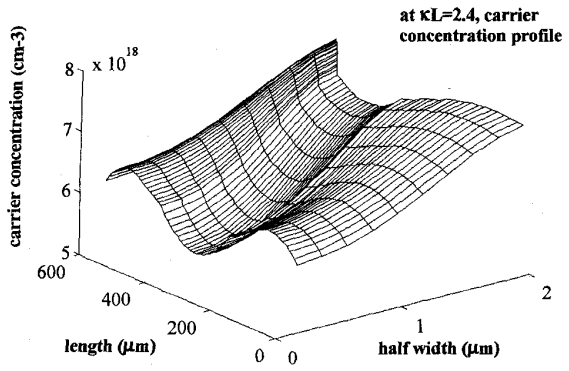

Fig. 12. The steady-state lateral and longitudinal carrier concentration distribution of DFB laser with double tapered wavegudie structure and $\kappa L = 2.4$.

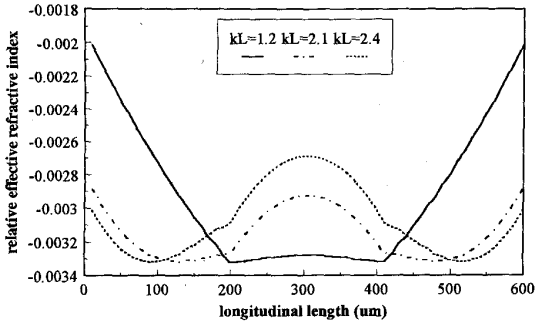

Fig. 13. The corresponding steady-state longitudinal effective refractive index profile of DFB laser with double tapered waveguide structure of Fig. 11.

device is also shown in Fig. 13. The refractive index profile is smoothly distributed along the longitudinal direction and this is different to that given in Fig. 8 (in Fig. 8, the refractive index profile has a step change along the length of waveguide). Stable and single longitudinal mode operation is the result of relatively uniform refractive index distribution.

V. Conclusion

A new quasi-three-dimensional large-signal dynamic model is developed for the analysis of combined lateral and longitudinal spatial hole burning effects on the dynamic response of DFB lasers. In addition, this model is also capable of including the lateral and longitudinal variations of optical field distribution. This model combines the beam-propagation method and the time-domain algorithm for solving the transient response of the coupled field equations and the rate equation of carrier distribution in a self-consistent manner. In the model, nonuniform distribution of spontaneous emission noise, nonuniform carrier injection and refractive index distribution are also taken into consideration.

Using this model, we analysis the influence of phase-adjustment region on the static and dynamic behavior of DFB lasers. It is shown that DFB lasers with wide-phase-adjustment region can enhance the stability of lateral mode, but for large κL ($\geq$2.4) longitudinal side modes are exhibited due to the severe longitudinal spatial hole burning near the phase adjustment region. On the other hand, for devices with narrow phase adjustment region and large κL, single-longitudinal mode is maintained due to the relatively uniform refractive index distribution along the longitudinal direction of the laser, but lateral side mode is excited for the reason of severe lateral spatial hole burning at the waveguide region. Furthermore, it is found that lasers with large κL and narrow phase adjustment region exhibit higher relaxation oscillation frequency than other devices' structure.

We proposed a DFB laser with double tapered waveguide structure. It is shown that the longitudinal and lateral spatial hole burning is minimized by the double tapered waveguide structure and stable-single-mode operation can be maintained. In addition, the power density at the facets is reduced by the wide stripe width. Therefore, the facets degradation by heating effects can be minimized. This device structure can be utilized to implement single-mode high-power semiconductor laser.

Acknowledgment

The author is very grateful to Mr. Wong Pak Ho of HKUEEE for his computational work.

References

[1] H. J. Wünshe, U. Bandelow, and H. Wenzel, "Calculation of combined lateral and longitudinal spatial hole burning in λ/4 shifted DFB lasers," *IEEE J. Quantum Electron.*, vol. 29, no. 6, pp. 1751–1760, 1993.

[2] S. F. Yu, R. G. S. Plumb, L. M. Zhang, M. C. Nowell, and J. E. Carroll, "Large signal dynamic behavior of distributed feedback lasers including lateral effects," *IEEE J. Quantum Electron.*, vol. 30, no. 5, pp. 1740–1750, 1994.

[3] S. F. Yu and E. H. Li, "Effects of lateral modes on the static and dynamic behavior of buried heterostructure DFB lasers," in *IEE Proc. Optoelectron.*, vol. 142, no. 2, 1995, pp. 97–102.

[4] G. P. Agrawal, "Fast Fourier transform based beam propagation model for stripe geometry semiconductor lasers: Inclusion of axial effects," *J. Appl. Phys.*, vol. 56, pp. 3100–3109, 1984.

[5] J. Hong, W. P. Huang, and T. Makino, "Static and dynamic simulation for ridge-waveguide MQW DFB lasers," *IEEE J. Quantum Electron.*, vol. 31, no. 1, pp. 49–59, 1995.

[6] W. Streifer, D. R. Scifres, and R. D. Burnham, "Coupled wave analysis of DFB and DBR lasers," *IEEE J. Quantum Electron.*, vol. 13, pp. 134–141, 1977.

[7] A. M. J. Adams, *An Introduction to Optical Waveguides.* New York: Wiley, 1981, ch. 6.

[8] L. M. Zhang, S. F. Yu, M. C. Nowell, D. D. Marcenac, J. E. Carroll, and R. G. S. Plumb, "Dynamic analysis of radiation and side mode suppression in second order DFB laser using time domain large signal traveling wave model," *IEEE J. Quantum Electron.*, vol. 30, no. 6, pp. 1389–1365, 1994.

[9] R. S. Zory, Ed., *Quantum Well Lasers.* New York: Academic, 1993, ch. 1.

[10] F. Gonthier, A. Henault, S. Lacroix, R. J. Black, and J. Bures, "Mode coupling in nonuniform fibers: Comparison between coupled mode theory and finite difference beam propagation method simulation," *J. Opt. Soc. Am. B*, vol. 8, no. 2, pp. 416–421, 1991.

[11] H. Sode, Y. Kotaki, H. Sudo, H. Ishikawa, S. Yamakoshi, and H. Imai, "Stability in single longitudinal mode operation in GaInAsP/InP phase-adjusted DFB lasers," *IEEE J. Quantum Electron.*, vol. 23, no. 6, pp. 804–814, 1987.

[12] J. Kinoshita, K. Ohtsuka, H. Agatsuma, A. Tanaka, T. Matsuyama, A. Makuta, and H. Kobayashi, "Performance of 1.5 μm DFB lasers with a narrow stripe region," *IEEE J. Quantum Electron.*, vol. 27, no. 6, pp. 1759–1765, 1991.

[13] J. Major, S. O'Brien, V. Gulgazov, D. Welch, and R. Lang, "High power single mode AlGaAs distributed bragg reflector laser diodes operating at 856 nm," *Electron. Lett.*, vol. 30, pp. 496–497, 1994.

[14] D. Garbuzov, N. Antonishkis, N. Zhigulin, N. Il'igulin, A. Kochergin, D. Lifshitz, E. Rafailov, and M. Fuksman, "High-power buried InGaAsP/GaAs ($\lambda = 0.8$ μm) laser diodes," *Appl. Phys. Lett.*, vol. 62, no. 10, pp. 1062–1064, 1993.

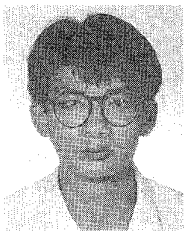

S. F. Yu received the B.Eng. degree (with Departmental Prize) in electronic engineering from London University, University College, England, in 1990 and the Ph.D. degree in optoelectronics from Cambridge University, Robinson College, England, in 1993.

He is a Fellow and Honorary Scholar of Cambridge Commonwealth trust and holds a Croucher Foundation scholarship while studying for the Doctoral program. In 1994, he joined the Department of Electrical and Electronic Engineering, University of Hong Kong, where he is a Lecturer. His main research topics include wavelength selectivity of grating coupled waveguides, transient properties of semiconductor laser diodes, and design of optoelectronic integrated circuit. He currently conducts the development of high-performance semiconductor lasers for the application in high-speed communication systems. He is also involved in the investigation of the influence of acoustic wave in semiconductor materials.